Load-dependent destabilization of the γ-rotor shaft in F_OF_1 ATP synthase revealed by hydrogen/deuterium-exchange mass spectrometry

Siavash Vahidi[a], Yumin Bi[b], Stanley D. Dunn[b,1], and Lars Konermann[a,b,1]

[a]Department of Chemistry, University of Western Ontario, London, ON, Canada N6A 5B7; and [b]Department of Biochemistry, University of Western Ontario, London, ON, Canada N6A 5C1

Edited by S. Walter Englander, Perelman School of Medicine, University of Pennsylvania, Philadelphia, PA, and approved January 12, 2016 (received for review October 15, 2015)

F_oF_1 is a membrane-bound molecular motor that uses proton-motive force (PMF) to drive the synthesis of ATP from ADP and P_i. Reverse operation generates PMF via ATP hydrolysis. Catalysis in either direction involves rotation of the γε shaft that connects the $\alpha_3\beta_3$ head and the membrane-anchored c_n ring. X-ray crystallography and other techniques have provided insights into the structure and function of F_oF_1 subcomplexes. However, interrogating the conformational dynamics of intact membrane-bound F_oF_1 during rotational catalysis has proven to be difficult. Here, we use hydrogen/deuterium exchange mass spectrometry to probe the inner workings of F_oF_1 in its natural membrane-bound state. A pronounced destabilization of the γ C-terminal helix during hydrolysis-driven rotation was observed. This behavior is attributed to torsional stress in γ, arising from γ···$\alpha_3\beta_3$ interactions that cause resistance during γ rotation within the apical bearing. Intriguingly, we find that destabilization of γ occurs only when F_oF_1 operates against a PMF-induced torque; the effect disappears when PMF is eliminated by an uncoupler. This behavior resembles the properties of automotive engines, where bearings inflict greater forces on the crankshaft when operated under load than during idling.

molecular motor | molecular bearing | conformational dynamics | destabilized helix | rotational resistance

Bacteria, mitochondria, and chloroplasts share a similar F_oF_1-ATP synthase architecture (1–3) (Fig. 1*A*). The *Escherichia coli* enzyme considered in this work has the rotor composition $\gamma\varepsilon c_{10}$ (4). The stator consists of the $\alpha_3\beta_3$ catalytic head, the δb_2 peripheral stalk, and the *a* subunit. The γε-rotor shaft connects $\alpha_3\beta_3$ with the ac_{10} proton translocator (3, 5). The intact molecular motor has a mass of 525 kDa. F_oF_1 investigations are typically conducted under hydrolysis conditions (1, 6, 7), where $\gamma\varepsilon c_{10}$ rotation is driven by the β subunits that cycle through a series of conformations (8). ATP hydrolysis triggers power strokes that involve consecutive interactions of the β-levers with γ (3, 6, 9).

X-ray crystallography (5, 8, 10, 11) and cryoelectron microscopy (12, 13) have provided valuable snapshots of subcomplexes and solubilized F_oF_1. Molecular dynamics (MD) simulations (14–16) can help interpret such data in a dynamic context. However, there is scant information on how the conformation of F_oF_1 is affected by internal and external forces while working under physiological conditions, where ATP/ADP interconversion is coupled with transmembrane proton transport in the presence of proton-motive force (PMF). With few exceptions (1, 3, 17), previous experiments on the rotary mechanism have focused on isolated F_1.

Of particular interest is the question of how moving protein surfaces within molecular motors interact with each other. The irregular topologies and specific binding interactions of biomolecular interfaces complicate a rigorous discussion of dissipative effects in terms of classical friction models (18). It seems likely that sliding motions at such interfaces will be associated with resistance as individual residues clash with one another, and as transient binding interactions are formed and disrupted (19). Rotation of γ within the $\alpha_3\beta_3$ apical bearing of F_oF_1 represents a prime example of such a scenario. Along these lines, recent MD simulations provided evidence for friction during torque-driven rotation of γ (15). More generally, both solvent friction and internal friction have been discussed in the context of conformational changes for monomeric proteins (19–21). For addressing these issues in the context of F_oF_1, it is necessary to interrogate the structure and dynamics of the molecular motor in situ while maintaining the system under different catalytically active and inhibited conditions.

Hydrogen/deuterium exchange (HDX) mass spectrometry (MS) is a sensitive approach for probing changes in protein structure and dynamics in response to external stimuli (22, 23). This technique monitors backbone deuteration in the presence of D_2O. Rigid protein segments exchange more slowly than regions that are not as structurally stable (24). Under continuous-labeling conditions, the deuteration kinetics can be monitored in a spatially resolved fashion by subjecting aliquots to peptic digestion, followed by liquid chromatography and MS analysis of the resulting peptides. The use of HDX/MS is well established for protein binding experiments and several other types of investigations (22, 23); however, this technique is underused for mechanistic studies on molecular machines (25). Ryrie and Jagendorf (26) monitored hydrogen/tritium exchange in chloroplast F_oF_1 four decades ago, but those experiments did not yield spatially resolved information.

Here, we use HDX/MS to compare the conformational dynamics of F_oF_1 under various catalytically active and inhibited conditions. The experiments were conducted using vesicles that represent the natural *E. coli* membrane environment. Our data

Significance

F_OF_1, or ATP synthase, is often referred to as the "world's smallest motor." Similar to automotive engines, it employs a rotating shaft that interacts with mechanical actuators. When operating a combustion engine under load, the bearings exert significant forces on the crankshaft, leading to enhanced mechanical stress. Here, we demonstrate that analogous load-dependent effects occur in molecular motors. When F_OF_1 pumps protons against a transmembrane gradient, the rotor shaft undergoes structural destabilization attributed to resistive forces in its apical bearing. The effect disappears when the transmembrane gradient opposing proton pumping is short-circuited by an uncoupler, as predicted by fundamental principles of mechanics. Our observations highlight fascinating parallels between engine operation on the macroscale and the nanoscale.

Author contributions: S.V., S.D.D., and L.K. designed research; S.V., Y.B., and S.D.D. performed research; Y.B. and S.D.D. prepared and characterized F_oF_1 membrane vesicles; S.V. and L.K. analyzed data; and L.K. wrote the paper.

The authors declare no conflict of interest.

This article is a PNAS Direct Submission.

[1]To whom correspondence may be addressed. Email: sdunn@uwo.ca or konerman@uwo.ca.

This article contains supporting information online at www.pnas.org/lookup/suppl/doi:10.1073/pnas.1520464113/-/DCSupplemental.

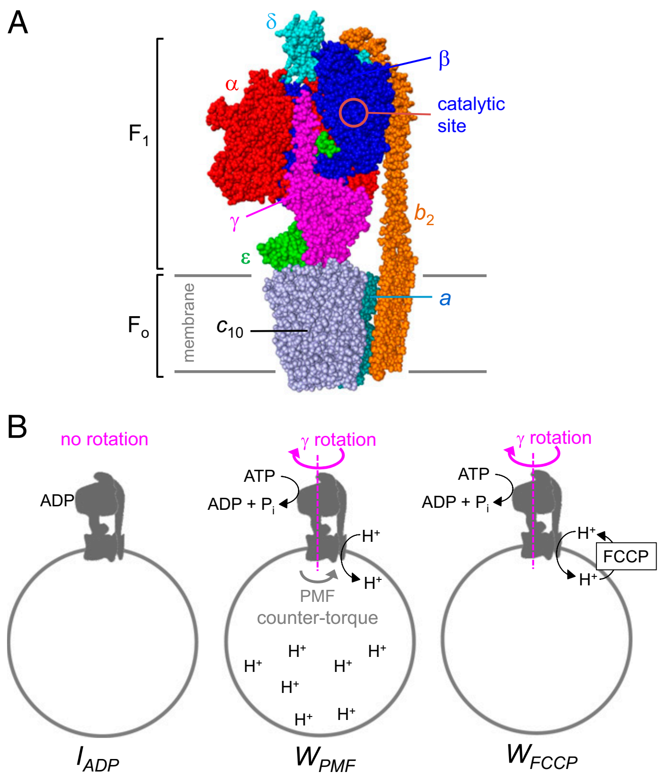

Fig. 1. Subunit architecture of F_oF_1 ATP synthase from *E. coli*. (*A*) Composite model assembled from subcomplex structures [Protein Data Bank (PDB) ID codes 3OAA, 3J0J, 1C17, 2XOK, and 2WSS]. One pair of αβ subunits facing the observer was removed to illustrate how γ extends into the apical bearing formed by the $\alpha_3\beta_3$ head. During rotational catalysis, ε (partially obstructed by γ) is likely folded down toward c_{10}, rather than being extended as shown here (10). (*B*) Cartoon of membrane vesicle-bound F_oF_1 under different experimental conditions. I_{ADP} represents ADP-inhibited F_oF_1; W_{PMF} represents catalytically active F_oF_1 that pumps protons against a PMF-mediated countertorque; and W_{FCCP} refers to catalytically active F_oF_1 that pumps protons in the presence of the uncoupler FCCP, which prevents PMF buildup.

reveal that the γ C-terminal helix experiences load-dependent destabilization. This effect reveals that rotation of the helix within the $\alpha_3\beta_3$ apical bearing is hindered by interchain contacts. We believe this investigation to be the first in situ HDX/MS investigation of a catalytically active rotational molecular motor.

Results and Discussion

HDX/MS of F_oF_1 in Membrane Vesicles. Deuteration measurements were conducted on F_oF_1 in inside-out *E. coli* membrane vesicles, with focus on three conditions (Fig. 1*B*): (*i*) The presence of ADP (without ATP) produces the inhibited state I_{ADP}, where Mg·ADP and azide remain permanently bound in at least one catalytic site (27); (*ii*) the W_{PMF} state is catalytically active ("working"; i.e., protons are pumped into the vesicle against PMF); and (*iii*) W_{FCCP} also represents catalytically active F_oF_1, but PMF buildup is prevented by the uncoupler carbonyl cyanide-4-(trifluoromethoxy) phenylhydrazone (FCCP). An ATP regeneration system was used to ensure that W_{PMF} and W_{FCCP} underwent ATP hydrolysis with $k_{cat} = 11 \pm 1\ s^{-1}$, resulting in ~30,000 catalytic events per enzyme during the 45-min HDX time window. This value corresponds to ~10,000 complete γ rotations for both W_{PMF} and W_{FCCP}, whereas rotation is blocked under I_{ADP} conditions.

Control measurements were extended to two additional types of samples: adenosine 5′-(β,γ-imido)triphosphate (AMP-PNP)–inhibited F_oF_1, as well as Mg^{2+}-depleted preparations (*SI Appendix*, Fig. S1). These control measurements confirmed that HDX/MS is capable of pinpointing changes in structure and dynamics of vesicle-bound F_oF_1 with high fidelity (*SI Appendix*, Fig. S1*A*).

The use of natural *E. coli* membranes resulted in peptic digests containing a large number of peptides from proteins other than F_oF_1. Ribosomal proteins, in particular, were present in high abundance, despite the use of sucrose gradient ultracentrifugation during membrane isolation (details are provided in *SI Appendix*, *Methods*). A multidimensional analysis work flow using peptide separation based on *m/z*, retention time, and ion mobility drift time was required to cope with these highly complex samples (*SI Appendix*, Fig. S2). These digestion and analysis conditions consistently yielded a total of 203 F_oF_1 peptides with signal-to-noise ratios that were adequate for providing highly reproducible HDX/MS data. Sequence coverage for the extramembrane subunits of F_oF_1 was high (α, 83%; β, 81%; γ, 74%; δ, 77%; ε, 48%; *b*, 58%). Unfortunately, only a few peptides were detected for membrane-embedded subunits, such that a meaningful characterization of *a* and *c* was not possible. Low digestion yields for transmembrane segments are common in HDX/MS (28). The use of natural membranes in this work is particularly challenging (29). Notably, most earlier membrane protein HDX/MS investigations used detergent-solubilized samples (30) or purified membrane surrogates, such as nanodiscs (31).

Deuteration Behavior of Selected Peptides. It is instructive to look initially at selected unprocessed HDX/MS data. The P-loop peptide β^{148}FGGAGVGKTVNM^{159} is involved in nucleotide binding (8). In the I_{ADP} state, this region displays asymmetrical HDX distributions (Fig. 2*A*) that are consistent with the three stable catalytic site conformations β_{tight}, β_{loose}, and β_{open} (32). We attribute the most extensively deuterated P-loop component to β_{loose}, which is known to adopt a distorted conformation with several disrupted H-bonds (8). Rotational averaging under W_{PMF} and W_{FCCP} conditions causes coalescence into a unimodal HDX envelope (Fig. 2*A*). Similar effects were observed for two other peptides close to the catalytic sites: β^{177}AGVGERTREGNDF^{189} and α^{360}FNAGIRPAVNPGIS^{373}. Regions that are insensitive to changes in conditions include the β-levers (Fig. 2*B*). The γ C-terminal helix shows greatly enhanced HDX for W_{PMF}, but not for W_{FCCP} or I_{ADP} (Fig. 2*C*). Results for ε are illustrated in *SI Appendix*, Fig. S3.

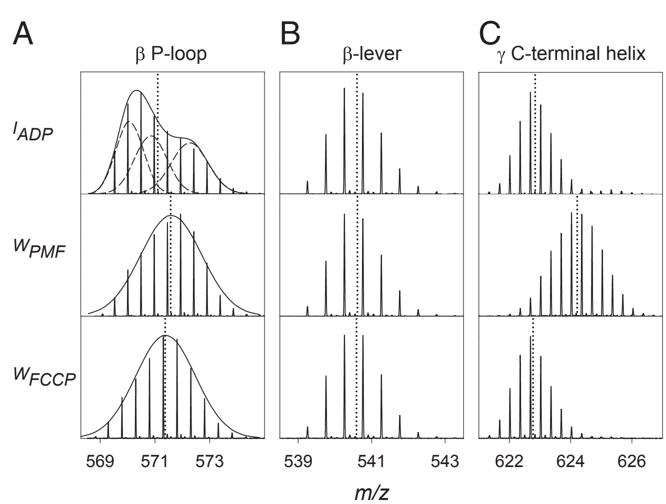

Fig. 2. HDX mass spectra of selected peptides in the I_{ADP}, W_{PMF}, and W_{FCCP} states. (*A*) Data for a peptide comprising the active site P-loop (β^{148}FGGAGVGKTVNM^{159}) after 1.5 min of deuteration. Gaussian deconvolution of the I_{ADP} spectrum reveals the presence of three equally populated noninterconverting conformers, attributed to β_{tight}, β_{loose}, and β_{open}. (*B*) β-Lever region (β^{380}DELSEEDKL^{388}) at $t = 45$ min. (*C*) γ C-terminal region (γ^{260}LQLVYNKARQASITQE^{275}) at $t = 45$ min. Vertical dotted lines represent centroid *m/z* values.

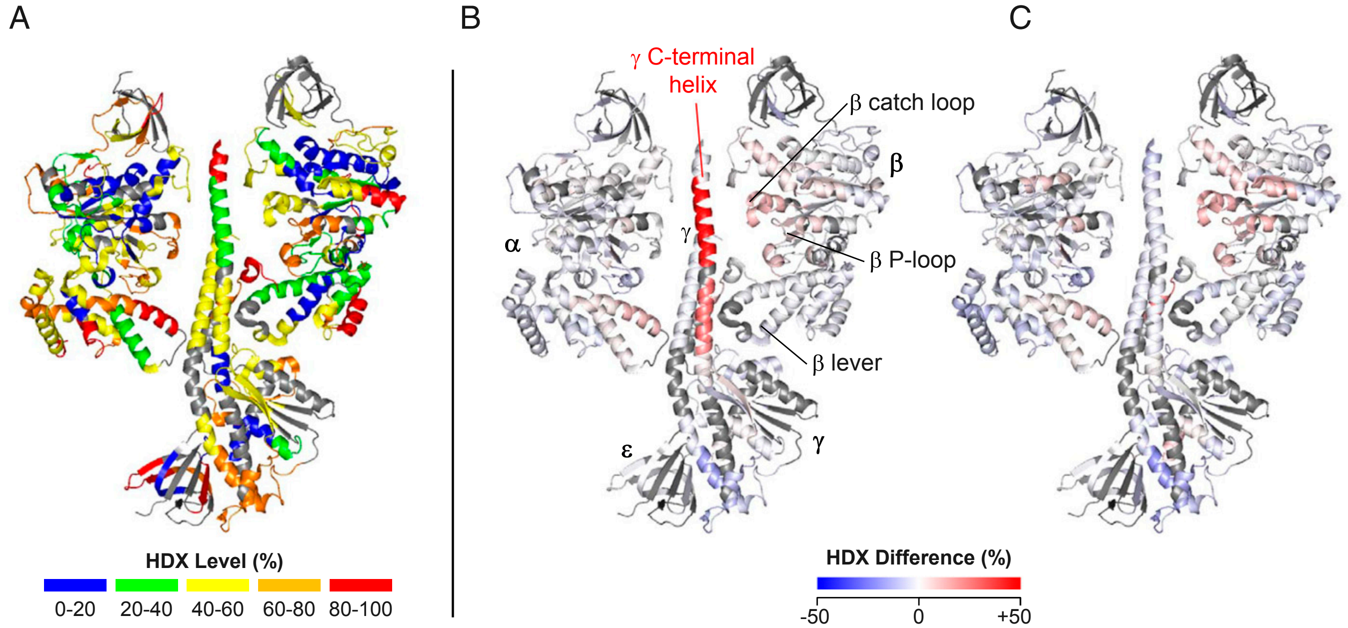

Fig. 3. (*A*) HDX levels of I_{ADP} for an HDX period of 45 min. Colors represent deuteration percentages as indicated in the legend; these data were derived from the centroids of the corresponding isotope distributions. To simplify the graphic representation, this figure only displays HDX/MS data for one α subunit and one β subunit, as well as γ and ε (PDB ID code 3OAA). (*B*) Deuteration difference map of W_{PMF} vs. I_{ADP}. (*C*) Deuteration difference map of W_{FCCP} vs. I_{ADP}. Dark red coloring of the γ C-terminal helix in *B* highlights dramatically enhanced deuteration of γ^{260}LQLVYNKARQASITQEL^{276} under W_{PMF} compared with I_{ADP} conditions. Regions not covered by peptide mapping are shown in dark gray.

Comprehensive Overview of HDX Patterns. For discussing the HDX properties of F_oF_1, it is convenient to adopt I_{ADP} as a reference state (Fig. 3*A*), yielding the difference maps of Fig. 3 *B* and *C*. W_{PMF} conditions are known to induce elastic deformation of the γ globular bottom domain (33), because the β-lever action is opposed by a c_{10} countertorque (3). For W_{FCCP}, this mechanical stress is greatly reduced because the c_{10} countertorque is eliminated. These considerations suggest that F_oF_1 power transmission elements might exhibit PMF-dependent HDX characteristics. Unexpectedly, Fig. 3 *B* and *C* reveals that the HDX behavior of key power transmission elements [γ bottom domain and β-levers (3)] is largely identical with and without PMF (Fig. 3 *B* and *C*). We conclude that much of the F_oF_1 H-bonding network resists perturbation by intramolecular forces encountered during rotational catalysis.

Interestingly, major PMF-dependent HDX changes are seen for parts of the γ C-terminal helix, with deuteration levels that are ∼40% higher under W_{PMF} conditions than in the W_{FCCP} and I_{ADP} states (Figs. 3 *B* and *C* and 4). This effect is most pronounced for the range γ^{260}LQLVYNKARQASITQEL^{276}, which appears in dark red in Fig. 3*B*. The corresponding region is covered by five partially overlapping peptides (*SI Appendix*, Fig. S5). The greatly enhanced deuteration of this γ region reveals the occurrence of structural perturbations when rotational catalysis proceeds in the presence of PMF (Fig. 3*B*). No such destabilization is observed when the rotor shaft is stationary (I_{ADP}) or when rotation takes place in the absence of PMF (W_{FCCP}; Fig. 3*C*).

Characterizing the Structure of PMF-Destabilized γ. For exploring the nature of PMF-induced structural perturbations in the γ C-terminal helix, it is helpful to consider the deuteration behavior of γ in the context of classical HDX theory (24, 34, 35). Backbone NH groups in regions that are permanently disordered are known to undergo rapid HDX with an overall rate constant k_{HDX} that approaches the "chemical" rate constant of $k_{ch} \approx 30\ \mathrm{s}^{-1}$ at pD 8 (35). Such rapid deuteration causes a burst phase in continuous labeling experiments. This behavior is displayed by the extreme C terminus of γ (^{279}IVSGAAAV^{286}; Fig. 4*B*), which shows a burst amplitude of ∼70%. In other words, γ^{279}IVSGAAAV^{286} is largely disordered in solution, regardless of experimental conditions.

Deuteration of amide NH groups in folded regions is mediated by transient H-bond opening/closing fluctuations, as envisioned by the native state mechanism (24, 35):

$$NH_{closed} \underset{k_{cl}}{\overset{k_{op}}{\rightleftharpoons}} NH_{open} \xrightarrow[D_2O]{k_{ch}} exchanged,$$

where $k_{cl} >> k_{op}$. In the EX2 regime encountered here, the resulting overall rate constant is $k_{HDX} = (k_{op}/k_{cl}) \times k_{ch}$ and the free energy associated with H-bond opening is $\Delta G^\circ = -RT\ln(k_{HDX}/k_{ch})$. Amides that follow this native state mechanism do not show a burst phase (i.e., deuteration for short HDX times is close to zero). For extremely stable regions, k_{op}/k_{cl} is so small that deuteration remains virtually undetectable throughout the entire experimental time window. Such a case is encountered for γ^{149}IGPVKVML^{156}, which is part of the globular γ bottom domain (Fig. 4*D*).

The γ C-terminal helix region that undergoes PMF-dependent destabilization (γ^{260}LQLVYNKARQASITQEL^{276}) shows deuteration kinetics in-between these two extremes (Fig. 4*C*). None of the profiles in Fig. 4*C* exhibits a burst phase, implying that residues γ 260–276 remain predominantly folded, with occasional H-bond opening/closing transitions. These transient opening events are much more extensive under W_{PMF} conditions than for W_{FCCP} and I_{ADP}. The heavy extent of deuteration and greatly increased HDX rate of W_{PMF} are readily apparent in Fig. 4*C*. The k_{HDX} values estimated from the exponential fits of Fig. 4*C* imply that hydrogen bonds in this region get destabilized by ∼4 kJ·mol^{-1} (1–2 k_BT) on average, from $\Delta G^\circ \approx 32$ kJ·mol^{-1} in the W_{FCCP} state to 28 kJ·mol^{-1} per hydrogen bond under W_{PMF} conditions.

Evidence for Hindered Rotation of γ. What causes the destabilization of the γ C-terminal helix? Any mechanistic explanation has to address the observation that rotation, per se, is insufficient for causing this destabilization (W_{FCCP}; Fig. 3*C*). Instead, destabilization is observed only when F_oF_1 operates against a PMF-mediated countertorque

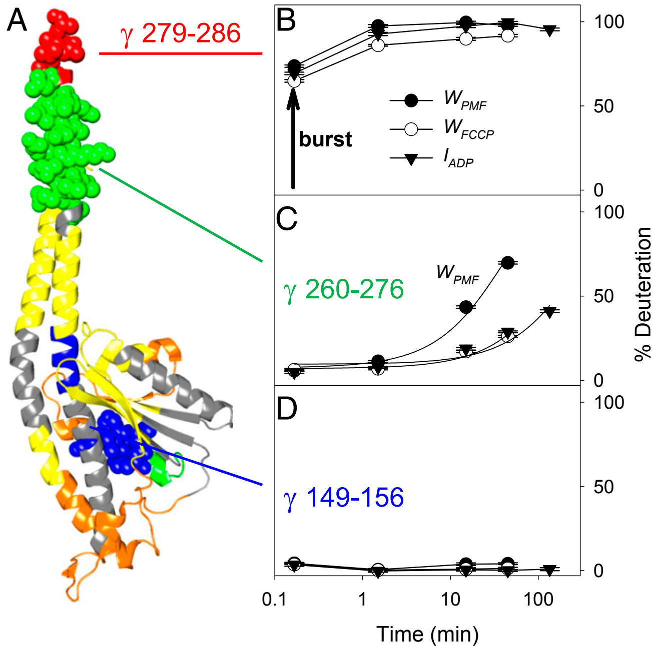

Fig. 4. Deuteration behavior of selected γ segments. (*A*) X-ray structure of γ, colored as in Fig. 3*A*. Three peptides are highlighted in space-fill representation: γ[279]IVSGAAAV[286], γ[260]LQLVYNKARQASITQEL[276], and γ[149]IGPVKVML[156]. (*B–D*) HDX kinetics of these peptides are shown for I_{ADP}, W_{PMF}, and W_{FCCP} conditions. Lines in *C* are single-exponential fits, subject to the constraint that the deuteration level for $t = \infty$ is 100%. The corresponding rate constants are 6×10^{-5} s^{-1}, 46×10^{-5} s^{-1}, and 9×10^{-5} s^{-1}, respectively. The vertical arrow in *B* represents burst phase labeling with an amplitude of ∼70%.

(W_{PMF}; Fig. 3*B*). Different reasons may be considered when trying to account for this behavior:

i) Direct power transmission: The most strongly destabilized region (Fig. 3*B*, dark red) is not directly involved in β/γ power transmission (3, 36, 37). Even F_oF_1 constructs with severely truncated γ C termini can still generate significant torque (36, 38, 39). Those previous findings imply that the PMF-induced destabilization of the γ C-terminal helix seen in our experiments is not a direct power transmission effect.

ii) Reverse rotation during dwell periods: Individual power strokes cause γ to turn 120° in a clockwise direction, when viewed from the top of the $\alpha_3\beta_3$ crown (40). Each power stroke is followed by a dwell, during which none of the β-levers actively drives γ rotation (6). One may contemplate whether PMF can cause reverse (counterclockwise) rotation of c_{10} by a small angle (<<120°) during these dwells, as suggested by some early experiments (41). Could such reverse rotation events destabilize the γ C-terminal helix? The $\gamma\varepsilon c_{10}$ rotor is remarkably compliant ("soft") in the globular bottom domain of γ, as required for elastic power transmission (3). Small reverse rotation events would likely be absorbed in this compliant region, such that their effects would not be felt at the opposite end of γ. Thus, it appears implausible that reverse rotation events could be responsible for the PMF-dependent destabilization of the γ C-terminal helix.

iii) Permanent stalling of the γ C terminus: Hilbers et al. (37) demonstrated that rotational catalysis proceeds unimpeded in F_1 constructs that had the γ C terminus cross-linked with α via an engineered disulfide bridge. In those constructs, the torque provided by $\alpha_3\beta_3$ permanently unfolds parts of the γ C-terminal helix, causing γ to undergo ϕ/ψ swivel motions instead of rotating as a whole (37). One has to consider the possibility that comparable effects are encountered for wild-type F_oF_1 in our W_{PMF} experiments, (i.e., complete stalling of the γ C terminus and unraveling of the γ C-terminal helix). Catalysis in the cross-linked constructs of Hilbers et al. (37) proceeds with permanent opening of approximately eight H-bonds in the γ C-terminal region. Such a situation would cause an HDX burst phase. The absence of a burst in Fig. 4*C* argues against permanent unfolding, making it unlikely that PMF induces complete stalling of the γ C terminus in our experiments. The work of Hilbers et al. (37) nonetheless provides important clues for the current discussion. Specifically, one can consider a scenario where γ is not permanently stalled, but experiences hindrance as the C-terminal helix rotates within the $\alpha_3\beta_3$ apical bearing. In the following section, we make the case that such a model is consistent with our data.

iv) Rotational resistance in the apical bearing: The movement of closely spaced protein surfaces relative to each other is accompanied by side-chain clashes and transient binding/dissociation events (19), likely giving rise to intermittent motion in a stick-slip regime (18). MD simulations indicate that such friction-like effects are also encountered during rotation of the γ C-terminal helix within the $\alpha_3\beta_3$ apical bearing (15). The simulated γ rotation in the study by Okazaki and Hummer (15) is orders of magnitude faster than in our experiments, thereby complicating comparisons of the data obtained. Nonetheless, our findings support the basic conclusion of Okazaki and Hummer (15) that rotation of γ is associated with mechanical resistance. The F_oF_1 apical bearing region is highlighted in Fig. 5*A*; it includes the sleeve surrounding the extreme γ C terminus (8), as well as adjacent elements, such as the β-catch loops (42, 43). Rotation will be accompanied by steric clashes as γ side chains are forced past the side chains of $\alpha_3\beta_3$ within the tight annular gap of the bearing (15). Intermolecular H-bonds and other noncovalent $\gamma\cdots\alpha_3\beta_3$ linkages (43, 44) may amplify these resistive effects. Fig. 5*B* illustrates how the resulting resistive forces (F_R, purple) will hinder rotation of γ. These F_R oppose the β-lever force (F_β, blue), thereby causing overtwisting of the γ C-terminal helix. The torsional stress generated under these conditions will destabilize backbone H-bonds such that HDX rates are enhanced (Fig. 5*B*). Protein-protein contacts will also hinder

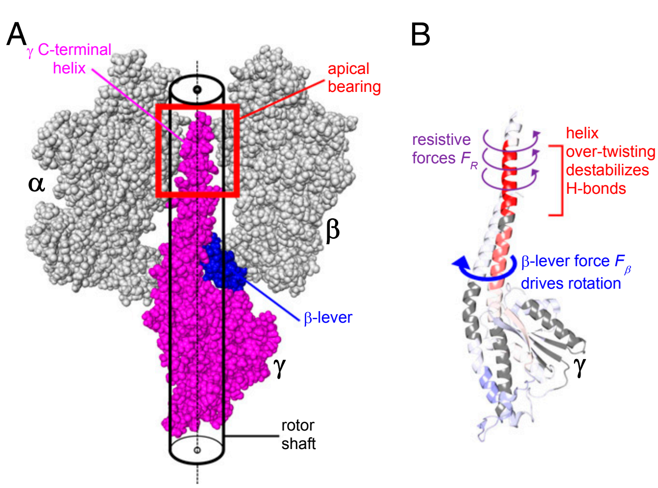

Fig. 5. (*A*) Close-up view of $\gamma/\alpha_3\beta_3$ contacts (PDB ID code 3OAA after hydrogen addition; only one αβ pair is shown). Surface roughness in the apical bearing causes F_R during γ rotation. (*B*) Interplay between F_R exerted by the apical bearing and F_β induces torsional stress in the γ C-terminal helix during each power stroke. We propose that this torsional stress destabilizes H-bonds, and thereby accelerates HDX in this region. The coloring of γ in *B* is consistent with the coloring of γ in Fig. 3*B*.

rotation elsewhere along the shaft, but the apical region is most vulnerable because the apical region is where γ tapers from a coiled coil into a single helix.

Scenario *iv* where γ encounters rotational resistance can explain the observed PMF dependence. An eccentric force acting on a shaft results in a stable rotation axis only if the shaft is supported by suitable bearings (45). This general principle applies equally to piston-driven crankshaft rotation and to β-lever–driven γ rotation in F_oF_1. Combustion engine measurements revealed that forces exerted by bearings on the crankshaft are much greater under load than during idling (45). Surface protrusions on either side of the bearing/shaft interface are more likely to interact with each other in the presence of a load, where the pressure inside the bearing is significantly enhanced (45, 46). In extreme cases, these interactions can induce material degradation (46). Our HDX data suggest that analogous effects are experienced by the γ-rotor shaft. The apical $\alpha_3\beta_3$ bearing will exert greater mechanical pressure on the γ C-terminal helix in the presence of a PMF load. This bearing pressure will promote interlocking of side chains in the annular gap, thereby enhancing F_R (purple arrows in Fig. 5*B*). As indicated in Fig. 5*B*, the resulting interplay of F_R and F_β causes overtwisting of the γ C-terminal helix during each power stroke, thereby destabilizing H-bonds and increasing HDX rates. Bearing pressure is lower in the absence of PMF, such that contacts at the $\gamma/\alpha_3\beta_3$ interface become less tight. The resulting drop in F_R diminishes the extent of helix overtwisting during power strokes, thereby lowering HDX levels under W_{FCCP} conditions. A semiquantitative framework that further dissects the interplay between PMF and γ overtwisting is outlined in *SI Appendix*, Fig. S6.

In summary, the PMF-induced destabilization of the γ C-terminal helix is a nontrivial phenomenon. Of all the explanations considered above, scenario *iv* is the most plausible one. It attributes the observed destabilization to rotational resistance, consistent with crystallographically detected contacts between γ and $\alpha_3\beta_3$ (43, 44), and with nonspecific friction seen in MD simulations (15).

Conclusions

F_oF_1-ATP synthase in a cellular environment normally operates in the presence of PMF. Thus, the findings of this work imply that a certain degree of rotational resistance is intrinsic to F_oF_1 operation in vivo. Our experiments could only explore ATP hydrolysis-driven rotation, but resistance will likely also be encountered during ATP synthesis.

The HDX kinetics indicate that ∼16 hydrogen bonds in the γ C-terminal region of F_oF_1 become destabilized by ∼4 $kJ\cdot mol^{-1}$ under W_{PMF} conditions, corresponding to an overall free energy "penalty" of ∼64 $kJ\cdot mol^{-1}$, which is roughly equivalent to the hydrolysis of two ATP molecules (3). Evidently, it is impossible that this amount of free energy is invested during each single ATP hydrolysis event, or during each 360° rotation of γ. Instead, we propose that this 64 $kJ\cdot mol^{-1}$ destabilization reflects accumulated torsional stress in γ that builds up gradually and that persists over extended time periods while F_oF_1 is catalytically active. In other words, the rotational resistance encountered under W_{PMF} conditions prevents γ from returning to a torsionally relaxed conformation between power strokes. This scenario is consistent with the well-established view that torsional elasticity allows γ to serve as an energy reservoir (3, 33). The functional significance of strong interactions in the apical bearing is revealed by the findings that disruption of contacts in this region by either truncation of γ or specific amino acid changes to β or γ impairs or prevents ATP-dependent H^+-pumping in membrane vesicles and oxidative phosphorylation in vivo (42, 43, 47).

Experiments on isolated F_1 suggest a catalytic efficiency close to 100% (3, 48). Other data indicate that the efficiency is somewhat lower (6), leaving room for dissipative phenomena. Our proposal of persisting torsional stress in the γ C-terminal helix is consistent with highly efficient operation of F_oF_1. The total free energy converted by each F_oF_1 enzyme in our experiments (with 30,000 turnover events) is $\sim 10^6$ $kJ\cdot mol^{-1}$. Thus, the percentage of free energy associated with torsional stress accumulation is negligibly small (on the order of 64 $kJ\cdot mol^{-1}/10^6$ $kJ\cdot mol^{-1}$).

Wild-type F_oF_1 under W_{PMF} conditions shares interesting parallels with the disulfide constructs used by Hilbers et al. (37), although the extent of the effects encountered in either case is different: (*i*) W_{PMF} experiences mechanical resistance during rotation of the γ C-terminal helix, whereas the disulfide constructs operate with a permanently stalled γ C terminus; (*ii*) rotational obstacles in W_{PMF} give rise to structural destabilization of the γ C-terminal helix, whereas the disulfide constructs experience complete unfolding of a large helix segment; and (*iii*) W_{PMF} conditions carry a moderate free energy penalty of ∼64 $kJ\cdot mol^{-1}$, but the persisting nature of the structural destabilization allows wild-type F_oF_1 to perform highly efficient catalysis. Unraveling of the helix in the disulfide constructs carries a very large free energy penalty that does not interfere with catalysis due to the persisting nature of the structural change (the helix does not refold after the initial unraveling event). Overall, the behavior displayed by the permanently stalled constructs of Hilbers et al. (37) bolsters the validity of our conclusions; their study demonstrates that efficient catalysis is possible even under conditions that are much more severe than the gentle rotational resistance deduced from our HDX/MS data for wild-type W_{PMF}.

The load-dependent rotor destabilization seen here for γ represents a prototypical power train feature (45, 46). Our findings highlight the fact that rotor bearings in macroscopic engines and molecular motors share common operational features. HDX/MS is well suited for interrogating these and other aspects of protein-based nanomachines. In the future, it will be interesting to apply this approach to other types of molecular motors, including flagellar systems.

Methods

The deuteration kinetics of F_oF_1 were monitored under various inhibited (*I*) and working (*W*) conditions [I_{ADP}, W_{PMF}, W_{FCCP}, $I_{AMP\text{-}PNP}$, and the Mg^{2+}-depleted inhibited state ($I_{Mg\text{-}dep}$)]. Inside-out *E. coli* membrane vesicles were exposed to 90% D_2O-based labeling buffer. Aliquots were removed at various time points. Peptic digestion was carried out offline under acid-quench conditions, and peptides were separated using reverse-phase chromatography on a nanoAcquity UPLC system (Waters). Ion mobility separation and mass analysis were conducted on a Synapt G2 electrospray quadrupole time-of-flight mass spectrometer (Waters). Details regarding sample preparation and experimental methods are provided in *SI Appendix*.

ACKNOWLEDGMENTS. This work was supported by the Canadian Institutes of Health Research (Grant FRN 10237 to S.D.D.) and the Natural Sciences and Engineering Council of Canada (Grant DG 217080-2013 to L.K.).

1. Sielaff H, Borsch M (2013) Twisting and subunit rotation in single F(O)(F1)-ATP synthase. *Philos Trans R Soc B Biol Sci* 368(1611):20120024.
2. Wächter A, et al. (2011) Two rotary motors in F-ATP synthase are elastically coupled by a flexible rotor and a stiff stator stalk. *Proc Natl Acad Sci USA* 108(10):3924–3929.
3. Junge W, Nelson N (2015) ATP synthase. *Annu Rev Biochem* 84:631–657.
4. Ballhausen B, Altendorf K, Deckers-Hebestreit G (2009) Constant c10 ring stoichiometry in the Escherichia coli ATP synthase analyzed by cross-linking. *J Bacteriol* 191(7):2400–2404.
5. Symersky J, et al. (2012) Structure of the c(10) ring of the yeast mitochondrial ATP synthase in the open conformation. *Nat Struct Mol Biol* 19(5):485–491.
6. Martin JL, Ishmukhametov R, Hornung T, Ahmad Z, Frasch WD (2014) Anatomy of F1-ATPase powered rotation. *Proc Natl Acad Sci USA* 111(10):3715–3720.
7. Uchihashi T, Iino R, Ando T, Noji H (2011) High-speed atomic force microscopy reveals rotary catalysis of rotorless F_1-ATPase. *Science* 333(6043):755–758.
8. Abrahams JP, Leslie AGW, Lutter R, Walker JE (1994) Structure at 2.8 A resolution of F_1-ATPase from bovine heart mitochondria. *Nature* 370(6491):621–628.

9. Mnatsakanyan N, Krishnakumar AM, Suzuki T, Weber J (2009) The role of the beta-DELSEED-loop of ATP synthase. *J Biol Chem* 284(17):11336–11345.
10. Cingolani G, Duncan TM (2011) Structure of the ATP synthase catalytic complex (F_1) from *Escherichia coli* in an autoinhibited conformation. *Nat Struct Mol Biol* 18(6): 701–707.
11. Morales-Rios E, Montgomery MG, Leslie AGW, Walker JE (2015) Structure of ATP synthase from Paracoccus denitrificans determined by X-ray crystallography at 4.0 Å resolution. *Proc Natl Acad Sci USA* 112(43):13231–13236.
12. Baker LA, Watt IN, Runswick MJ, Walker JE, Rubinstein JL (2012) Arrangement of subunits in intact mammalian mitochondrial ATP synthase determined by cryo-EM. *Proc Natl Acad Sci USA* 109(29):11675–11680.
13. Allegretti M, et al. (2015) Horizontal membrane-intrinsic α-helices in the stator a-subunit of an F-type ATP synthase. *Nature* 521(7551):237–240.
14. Nam K, Pu J, Karplus M (2014) Trapping the ATP binding state leads to a detailed understanding of the F1-ATPase mechanism. *Proc Natl Acad Sci USA* 111(50): 17851–17856.
15. Okazaki K, Hummer G (2015) Elasticity, friction, and pathway of γ-subunit rotation in FoF1-ATP synthase. *Proc Natl Acad Sci USA* 112(34):10720–10725.
16. Mukherjee S, Warshel A (2015) Dissecting the role of the γ-subunit in the rotary-chemical coupling and torque generation of F1-ATPase. *Proc Natl Acad Sci USA* 112(9):2746–2751.
17. Sambongi Y, et al. (1999) Mechanical rotation of the c subunit oligomer in ATP synthase (F0F1): Direct observation. *Science* 286(5445):1722–1724.
18. Gangloff D, Bylinskii A, Counts I, Jhe W, Vuletic V (2015) Velocity tuning of friction with two trapped atoms. *Nat Phys* 11(11):915–919.
19. Soranno A, et al. (2012) Quantifying internal friction in unfolded and intrinsically disordered proteins with single-molecule spectroscopy. *Proc Natl Acad Sci USA* 109(44):17800–17806.
20. Chung HS, Eaton WA (2013) Single-molecule fluorescence probes dynamics of barrier crossing. *Nature* 502(7473):685–688.
21. Bieri O, et al. (1999) The speed limit for protein folding measured by triplet-triplet energy transfer. *Proc Natl Acad Sci USA* 96(17):9597–9601.
22. Pirrone GF, Iacob RE, Engen JR (2015) Applications of hydrogen/deuterium exchange MS from 2012 to 2014. *Anal Chem* 87(1):99–118.
23. Kaltashov IA, Bobst CE, Abzalimov RR (2013) Mass spectrometry-based methods to study protein architecture and dynamics. *Protein Sci* 22(5):530–544.
24. Englander SW, Mayne L, Krishna MMG (2007) Protein folding and misfolding: mechanism and principles. *Q Rev Biophys* 40(4):287–326.
25. Pan Y, Brown L, Konermann L (2011) Hydrogen exchange mass spectrometry of bacteriorhodopsin reveals light-induced changes in the structural dynamics of a biomolecular machine. *J Am Chem Soc* 133(50):20237–20244.
26. Ryrie IJ, Jagendorf AT (1971) An energy-linked conformational change in the coupling factor in chloroplasts. Studies with hydrogen exchange. *J Biol Chem* 246(11):3771–3774.
27. Bowler MW, Montgomery MG, Leslie AGW, Walker JE (2006) How azide inhibits ATP hydrolysis by the F-ATPases. *Proc Natl Acad Sci USA* 103(23):8646–8649.
28. Joh NH, et al. (2008) Modest stabilization by most hydrogen-bonded side-chain interactions in membrane proteins. *Nature* 453(7199):1266–1270.
29. Rey M, Forest E, Pelosi L (2012) Exploring the conformational dynamics of the bovine ADP/ATP carrier in mitochondria. *Biochemistry* 51(48):9727–9735.
30. West GM, et al. (2011) Ligand-dependent perturbation of the conformational ensemble for the GPCR β2 adrenergic receptor revealed by HDX. *Structure* 19(10): 1424–1432.
31. Hebling CM, et al. (2010) Conformational analysis of membrane proteins in phospholipid bilayer nanodiscs by hydrogen exchange mass spectrometry. *Anal Chem* 82(13):5415–5419.
32. Boyer PD (1997) The ATP synthase–a splendid molecular machine. *Annu Rev Biochem* 66:717–749.
33. Sielaff H, et al. (2008) Domain compliance and elastic power transmission in rotary F(O)F(1)-ATPase. *Proc Natl Acad Sci USA* 105(46):17760–17765.
34. Hvidt A, Nielsen SO (1966) Hydrogen exchange in proteins. *Adv Protein Chem* 21: 287–386.
35. Bai Y, Milne JS, Mayne L, Englander SW (1993) Primary structure effects on peptide group hydrogen exchange. *Proteins* 17(1):75–86.
36. Hossain MD, et al. (2006) The rotor tip inside a bearing of a thermophilic F1-ATPase is dispensable for torque generation. *Biophys J* 90(11):4195–4203.
37. Hilbers F, Junge W, Sielaff H (2013) The torque of rotary F-ATPase can unfold subunit gamma if rotor and stator are cross-linked. *PLoS One* 8(1):e53754.
38. Junge W, Sielaff H, Engelbrecht S (2009) Torque generation and elastic power transmission in the rotary F(O)F(1)-ATPase. *Nature* 459(7245):364–370.
39. Furuike S, et al. (2008) Axle-less F1-ATPase rotates in the correct direction. *Science* 319(5865):955–958.
40. Noji H, Yasuda R, Yoshida M, Kinosita K, Jr (1997) Direct observation of the rotation of F1-ATPase. *Nature* 386(6622):299–302.
41. Chang TM, Penefsky HS (1974) Energy-dependent enhancement of aurovertin fluorescence. An indicator of conformational changes in beef heart mitochondrial adenosine triphosphatase. *J Biol Chem* 249(4):1090–1098.
42. Greene MD, Frasch WD (2003) Interactions among gamma R268, gamma Q269, and the beta subunit catch loop of Escherichia coli F1-ATPase are important for catalytic activity. *J Biol Chem* 278(51):51594–51598.
43. Boltz KW, Frasch WD (2005) Interactions of gamma T273 and gamma E275 with the beta subunit PSAV segment that links the gamma subunit to the catalytic site Walker homology B aspartate are important to the function of Escherichia coli F1F0 ATP synthase. *Biochemistry* 44(27):9497–9506.
44. Bowler MW, Montgomery MG, Leslie AGW, Walker JE (2007) Ground state structure of F1-ATPase from bovine heart mitochondria at 1.9 A resolution. *J Biol Chem* 282(19): 14238–14242.
45. Kapulainen M, et al. (2014) Fibre optic sensors for long-term monitoring of oil film pressure in diesel engine main bearing. *Tribol Lett* 56(1):47–54.
46. Wang QA (1997) Seizure failure of journal-bearing conformal contacts. *Wear* 210(1-2): 8–16.
47. Iwamoto A, Miki J, Maeda M, Futai M (1990) H(+)-ATPase gamma subunit of Escherichia coli. Role of the conserved carboxyl-terminal region. *J Biol Chem* 265(9): 5043–5048.
48. Yasuda R, Noji H, Kinosita K, Jr, Yoshida M (1998) F1-ATPase is a highly efficient molecular motor that rotates with discrete 120 degrees steps. *Cell* 93(7):1117–1124.